Fines Deposition Dynamics in Gas–Liquid Trickle-Flow Reactors

Ion Iliuta, Faïçal Larachi, and Bernard P. A. Grandjean
Chemical Engineering Dept. & CERPIC, Laval University, Québec, G1K 7P4, Canada

Nonfilterable fines, such as incipient coke particles or fines naturally occurring in oil sands bitumen, are known to be responsible for the severe plugging during the flow of (fine) solid–liquid suspensions in cocurrent gas–liquid trickle-bed hydrotreating reactors. Accumulating fines in the porous medium causes pressure buildup, and thus the dropoff in hydrogen partial pressure in the bed, overutilizing recycling compressors and shortening the reactor operating cycles. In this work, a 1-D transient two-fluid hydrodynamic model based on the macroscopic volume-average form of the multiphase system transport equations is developed, analyzed, and validated experimentally. The model hypothesizes that plugging occurs via deep-bed filtration mechanisms. It incorporates physical effects of porosity and effective specific surface-area changes due to the capture of fines, inertial effects of phases, and coupling effects between the fines filter rate equation and interfacial momentum exchange force terms. It is tested in the trickle-flow regime for conditions mimicking a hydrotreating trickle-bed process with spherical and trilobe catalysts. To rationalize deep-bed filtration phenomena in trickle-flow reactors, parametric studies are carried out on the effects of liquid velocity and viscosity, gas density and velocity, and fines feed concentration, on the plugging dynamics.

Introduction

Trickle-bed reactors consist of fixed beds of catalyst pellets through which gas and liquid streams are allowed to flow cocurrently downwards. Depending on throughputs, trickle beds experience a variety of flow regimes. The low L/G ratios at which trickle beds are typically operated induce the so-called trickle-flow regime wherein the liquid flows as thin films over the catalyst while the gas flows as a continuous and separate phase in the available porous space. These reactors are used a great deal in the petroleum industry for hydrotreating a multitude of hydrocarbon feeds such as in hydrogenation of aromatics and heterocycles, porphyrin hydrodemetallization, resin and asphaltene de-aggregation, hydrodecarbonization, and oxygen, sulfur, and nitrogen selective removal (Le Page et al., 1990; Meyers, 1996).

Usually *nonfilterable* fine solid impurities, such as iron sulfides, sodium chloride, coke, organic precipitates, and sediments, either naturally occurring in the liquid feed or formed *in situ*, get trapped in the trickle-bed hydrotreaters (Narayan et al., 1997; Gray et al., 2002). This occasions bed plugging and initiates liquid maldistribution and pressure buildup. Disposal of preventive upstream sacrificial catalytic beds having coarse-size catalysts alleviates in part the plugging problem. However, small-size fines being difficult to trap in the sacrificial filter beds, contamination of the downstream units is usually unavoidable.

Current industry response is to leave the bed collecting fines until pressure climbs to a critical level, forcing reactor shutdown. Pressure buildup is not desirable because it entrains overexploitation of the recycling compressors and a collapse in hydrogen partial pressure at the reactor outlet. Since for hydrotreating catalysts, hydrogen often controls the overall reaction rate, pressure buildup causes a loss in reactor catalytic performance in addition to the loss in activity due to the physical blockage of active sites by the collector-captured fines. Catalyst replacement is often required well before the catalyst activity is exhausted, occasioning additional costs and a loss in the process competitiveness.

One option to prolong cycle periods of trickle beds between successive shutdowns is to tailor catalyst grains with specially designed geometry, for example, the CDS-NP maca-

Correspondence concerning this article should be addressed to F. Larachi.

roni catalyst series of the UOP RCD Unionfining process (Meyers, 1996). Another route to lower plugging proposes to chemically alter the surface of the fine particles by adsorbing solutes, such as surfactants or polymers. By forming layers with sterically repulsive forces these stabilize the liquid–solid suspension, inhibit deposition of fines, and repel plugging. This method has been tested by Gray and coworkers, who extensively studied the effects of adding asphaltene polymers to kaolin fines on the deposition rates in hydrotreated light gas oil using a model batch internally recirculating draft-tube porous bed (Wang et al., 1999, 2001).

Although relatively little effort has been made to study the deposition phenomena of fines in nonaqueous media in trickle-bed reactors and their hydrodynamics, similar problems have been extensively studied, mainly in the context of *single-phase* aqueous flows in deep-bed filtration (Herzig et al., 1970; O'Melia and Ali, 1978; Vigneswaran and Tulachan, 1988; Tien, 1989; Stephan and Chase, 2000; Ortiz-Arroyo et al., 2002). While it is expected that the same general governing hydrodynamic equations model the plugging in trickle beds and in granular filters (Narayan et al., 1997), there are few key distinctions. The size of solid particles (or collectors) and vessel in granular beds, and liquid hourly space velocity are much smaller than in trickle beds. In addition, in granular filters no gas phase is present. Depending on the importance of gas–liquid interactions, the presence of a flowing gas phase may profoundly modify the liquid holdup and liquid interstitial velocity, thus influencing the extent of deposition in the trickle bed. The throughputs of fluids differ substantially. In a trickle bed, gas and liquid velocities range typically from 0.05 m/s to 0.5 m/s and 0.001 m/s to 0.025 m/s, respectively. In granular filters, liquid velocities are generally far less than 0.001 m/s and Darcy's law typically applies to model the pressure buildup due to fine collection in deep-bed filtration. In trickle beds, the inertial effects are nonnegligible and the Darcy's law is inadequate at higher gas and liquid velocities (Sáez and Carbonell, 1985).

Despite the operational importance of the problem of fines, little systematic work has been done to understand the process of fines accumulation. There is a lack of descriptive and quantitative *reactor-scale* models that can be used for predicting the fate of trickle-bed hydrodynamics under filtration conditions and for planning strategies for minimizing the problem of plugging. It is therefore vital to gain new fundamental knowledge by tackling the complex hydrodynamics and surface phenomena involved in the plugging with fines of trickle beds, especially under the conditions of interest to the oil-refining industry. This contribution is offered as a step in that direction.

In this work, a one-dimensional two-fluid model based on volume-average mass and momentum balance equations and volume-average species balance equations for the fines is developed for the description of two-phase flow and space-time evolution of the deposition of fines in trickle-bed reactors under trickle-flow regime. The impact of fines is evaluated in terms of pressure drop rise as a function of the specific deposit (or time), as well as in terms of plugging patterns, for example, local porosity, and fine concentration vs. bed depth. The approach is validated using the experiments and observations of Gray et al. (2002), who studied experimentally the plugging of a cold-flow trickle-bed unit during the flow of kerosene–clay suspensions through spherical and trilobe catalyst-containing trickle beds. The effects of liquid superficial velocity and viscosity, gas superficial velocity and density, influent fines concentration, and deposit porosity on pressure buildup are also analyzed.

Governing Equations for the Fines Dynamics in Gas–Liquid Trickle Flow

A cocurrent downward gas–liquid trickle flow through a porous medium of uniform initial porosity ϵ^o and single-sized catalytic particles is considered. For each flowing phase, we shall assume *unidirectional*, isothermal, Newtonian, and passive (no chemical reaction) conditions. The liquid phase is considered as incompressible and the gas phase is assumed to be an ideal gas: $\rho_g = P/RT$. The gas/liquid/fine/porous medium multiphase system is viewed as a system of three interpenetrated continua: (1) a flowing gas phase; (2) a dilute *pseudohomogeneous* fluid phase consisting of the liquid and the seeding fines, henceforth referred to as *fluid*; (3) and a stationary *pseudocontinuous* solid phase made up of the packing particles—in this work referred to as *collectors*—constituting the clean porous medium, as well as of the fines that get captured onto their surface.

Further assumptions inherent to the formulation developed in this work are:

- The fluid properties, for example, density, viscosity, holdup, are equal to those of the embracing liquid (inlet fines volume fraction usually down to 0.1‰).
- The bed is fully wetted by the liquid (wetting efficiency equals 100%) so that no room is left for gas–solid contacting, that is, no direct gas–solid drag force on the packing surface.
- The two-phase flow is annular and completely separated.
- Each phase, that is, gas, fluid, and solid, behaves as a continuum so that the macroscopic differential balance equations can be applied; however, except for the solid mass conservation, the solid stress balance is not included in the present analysis.
- The coupling between the fluid and solid phases is monitored via the fines filter rate equation (Eq. 19) and the interfacial drag forces (Eqs. 13, 14).
- The fines seeded in the liquid are considered *single-sized*, with density ρ_f and diameter d_f.
- Reentrainment of the deposited fines due to hydrodynamic drag forces is not allowed.
- Bed plugging by the blocking and sieving modes (Tien and Payatakes, 1979; Choo and Tien, 1995a) does not take place.
- The filtration mechanism to occur is of the deep-bed filtration type and not of the cake filtration type (Wang et al., 1999); in other words, fine–fine attractive interactions within the fluid phase are assumed absent or at least small enough to preclude flocculation.
- The gas–liquid interface is impervious to the fines.
- The net sink in the fluid momentum balance due to the mass transfer of fines from the fluid to the collector is negligibly small.

The nonsteady-state model being developed for describing the deep-bed filtration of fines in the trickle-flow regime is based on the adaptation of the macroscopic volume-average form of the transport equations for multiphase systems

(Whitaker, 1973). The model equations consist of the conservation of volume, conservation of mass or continuity, and conservation of momentum for the gas and fluid phases, continuity for the solid stationary phase (that is, the fixed bed), and species balance for the fines undergoing displacement from the fluid phase to the solid phase.

Conservation of volume

$$\epsilon_\ell + \epsilon_g = \epsilon. \tag{1}$$

Continuity for the gas and fluid phases

$$\frac{\partial}{\partial t}\epsilon_g \rho_g + \frac{\partial}{\partial z}\epsilon_g \rho_g u_g = 0 \tag{2}$$

$$\frac{\partial}{\partial t}\epsilon_\ell \rho_\ell + \frac{\partial}{\partial z}\epsilon_\ell \rho_\ell u_\ell + \rho_f N = 0. \tag{3}$$

Continuity for the solid phase

$$\frac{\partial}{\partial t}\left[(1-\epsilon^o)\rho_s + (1-\epsilon_d)(\epsilon^o - \epsilon)\rho_f\right] = \rho_f N. \tag{4}$$

Species balance for the fines

$$\frac{\partial}{\partial t}\epsilon_\ell c + \frac{\partial}{\partial z}\epsilon_\ell c u_\ell + N = 0. \tag{5}$$

Momentum balance equations for the gas and fluid phases

$$\frac{\partial}{\partial t}\rho_g \epsilon_g u_g + u_g \frac{\partial}{\partial z}\epsilon_g \rho_g u_g = \epsilon_g \mu_g^e \frac{\partial^2}{\partial z^2}u_g - \epsilon_g \frac{\partial}{\partial z}P + \epsilon_g \rho_g g - F_{g\ell} \tag{6}$$

$$\frac{\partial}{\partial t}\rho_\ell \epsilon_\ell u_\ell + u_\ell \frac{\partial}{\partial z}\rho_\ell \epsilon_\ell u_\ell = \epsilon_\ell \mu_\ell^e \frac{\partial^2}{\partial z^2}u_\ell - \epsilon_\ell \frac{\partial}{\partial z}P + \epsilon_\ell \rho_\ell g + F_{g\ell} - F_{\ell s}. \tag{7}$$

Here P stands for pressure; ϵ_α, ρ_α, and u_α represent, respectively, the holdup, the density, and the longitudinal (interstitial) velocity of phase α (gas or fluid phases), while the subscripts s and f refer to the solid phase and fines, respectively; and $F_{\alpha\beta}$ represents the interfacial drag force per unit reactor volume exerted at the interface between mutually interacting α and β phases (gas, fluid, and solid phases). The α-phase effective viscosity, μ_α^e, which arises from the combination of the viscous and the pseudoturbulence stress tensors, is formulated as proposed by Dankworth et al. (1990). In addition, g is the acceleration due to gravity, ϵ is the local porosity at time t, ϵ^o is the initial "clean" bed porosity, ϵ^d is the fines deposit porosity, c is the local fines volumetric concentration, and N is the local filtration rate. Note that in the formulation of the momentum balance equations, the capillary pressure between phase ℓ and phase g is neglected.

The fines are imposed in the fluid influent stream as a step-increase function after abrupt rerouting from the steady-state "fines-free" two-phase flow through the clean porous medium. Solution of this initial state is obtained by solving for $c = 0$ and $N = 0$ the conservation of volume, the conservation of mass and momentum for the gas, and the unloaded liquid.

Conservation of volume

$$\epsilon_\ell^o + \epsilon_g^o = \epsilon^o. \tag{8}$$

Continuity for the gas and unloaded liquid phases

$$\frac{\partial}{\partial t}\epsilon_g^o \rho_g + \frac{\partial}{\partial z}\epsilon_g^o \rho_g u_g^o = 0 \tag{9}$$

$$\frac{\partial}{\partial t}\epsilon_\ell^o \rho_\ell + \frac{\partial}{\partial z}\epsilon_\ell^o \rho_\ell u_\ell^o = 0. \tag{10}$$

Momentum balance equations for the gas and unloaded liquid phases

$$\frac{\partial}{\partial t}\rho_g \epsilon_g^o u_g^o + u_g^o \frac{\partial}{\partial z}\epsilon_g^o \rho_g u_g^o = \epsilon_g^o \mu_g^e \frac{\partial^2}{\partial z^2}u_g^o - \epsilon_g^o \frac{\partial}{\partial z}P + \epsilon_g^o \rho_g g - F_{g\ell}^o \tag{11}$$

$$\frac{\partial}{\partial t}\rho_\ell \epsilon_\ell^o u_\ell^o + u_\ell^o \frac{\partial}{\partial z}\epsilon_\ell^o \rho_\ell u_\ell^o = \epsilon_\ell^o \mu_\ell^e \frac{\partial^2}{\partial z^2}u_\ell^o - \epsilon_\ell^o \frac{\partial}{\partial z}P + \epsilon_\ell^o \rho_\ell g + F_{g\ell}^o - F_{\ell s}^o, \tag{12}$$

where the superscript o stands for the clean-bed flow and state.

To make the system solvable, the conservation equations (Eqs. 1–7) for the seven unknowns, that is, ϵ_ℓ, ϵ_g, ϵ, u_ℓ, u_g, P, and c, must be augmented by three auxiliary closure relations, namely, the gas–liquid, $F_{g\ell}$, the liquid–solid, $F_{\ell s}$, interfacial drag forces, and the filtration rate, N.

Closures for the Interfacial Drag Forces

In the momentum balance equations (Eqs. 6, 7, 11, 12), a set of constitutive equations is required for the interfacial drag forces. The assumption of full bed wetting entrains that the gas-phase drag will only have contributions due to effects located at the gas–liquid interface. The result of these forces, denoted $-F_{g\ell}$, is the drag force exerted on the gas phase as a result of the relative motion between the flowing phases to oppose slip. Similarly, the result of the forces exerted on the liquid (or fluid) involves two components: (1) the drag force, $-F_{\ell s}$, experienced by the liquid due to the shear stress near the liquid–solid boundary, and (2) the gas–liquid interfacial drag, $F_{g\ell}$.

It has been shown that under certain conditions the slit flow approximation yields a very satisfactory set of constitutive equations for the gas–liquid and the liquid–solid drag forces (Holub et al., 1992; Iliuta et al., 2000). The slit flow becomes well representative of the trickle-flow regime when the liquid texture is mainly contributed by collector-supported liquid films and rivulets, and the gas–liquid separated flow assumption holds. This generally occurs at small liquid irrigation rates that allow the transport of liquid in the form of a smooth and stable film (Holub et al., 1992). The actual

trickle-flow structure being conceptualized via an idealized gas–liquid (inclined) slit flow, the force balance equations for the gas and the clean (or fines-free) liquid, are first solved in the slit scale, and, from there, mapped into the bed scale. Using the available experimental pressure drop and liquid holdup data in the trickle-flow regime (ca. 5000 measurements collected from 42 sources), Iliuta et al. (2002) identified and validated the expressions for the liquid–solid and the gas–liquid drag forces. We will employ these closure expressions for the purpose of the present work, although there is no restriction keeping other constitutive formulations from being chosen instead (Sáez and Carbonell, 1985; Holub et al., 1992; Attou et al., 1999; Propp et al., 2000; Iliuta et al., 2000; Fourar et al., 2001). At a given depth z in the bed, the projections of the drag forces take the following forms

$$F_{\ell s}=\left\{\frac{E_1}{36}C_w^2a_{cf}^2\frac{(1-\epsilon)^2}{\epsilon_\ell^3}\mu_\ell+\frac{E_2}{6}C_{wi}(1+\psi_{g\ell})\times a_{cf}\frac{(1-\epsilon)}{\epsilon_\ell^3}\rho_\ell|v_\ell|\right\}v_\ell\epsilon_\ell \quad (13)$$

$$F_{g\ell}=\left\{\frac{E_1}{36}C_w^2a_{cf}^2\frac{(1-\epsilon)^2}{\epsilon_g^3}\mu_g+\frac{E_2}{6}C_{wi}(1+\psi_{g\ell})\times a_{cf}\frac{(1-\epsilon)}{\epsilon_g^3}\rho_g|v_g-\epsilon_g u^*|\right\}(v_g-\epsilon_g u^*)\epsilon_g, \quad (14)$$

whereas in the clean-bed case, the liquid–solid and gas–liquid drag forces needed in Eqs. 8–12 simplify to

$$F_{\ell s}^o=\left\{E_1C_w^2\frac{(1-\epsilon^o)^2}{(d_c^o)^2(\epsilon_\ell^o)^3}\mu_\ell+E_2C_{wi}(1+\psi_{g\ell})\times\frac{(1-\epsilon^o)}{d_c^o(\epsilon_\ell^o)^3}\rho_\ell|v_\ell^o|\right\}v_\ell^o\epsilon_\ell^o \quad (15)$$

$$F_{g\ell}^o=\left\{E_1C_w^2\frac{(1-\epsilon^o)^2}{(d_c^o)^2(\epsilon_g^o)^3}\mu_g+E_2C_{wi}(1+\psi_{g\ell})\times\frac{(1-\epsilon^o)}{d_c^o(\epsilon_g^o)^3}\rho_g|v_g^o-\epsilon_g^o u^*|\right\}(v_g^o-\epsilon_g^o u^*)\epsilon_g^o. \quad (16)$$

Here v_ℓ and v_g are the superficial velocities of the flowing phases based on the total cross-sectional area of the reactor; E_1 and E_2 are the bed Ergun viscous and inertial constants; and C_w and C_{wi} are the wall correction functions introduced here for, respectively, the viscous and the inertial terms. These can be evaluated using the functions defined by Liu et al. (1994)

$$C_w=1+\frac{\pi d_c^o}{6(1-\epsilon^o)D},\quad C_{wi}=1-\frac{\pi^2d_c^o}{24D}\left(1-\frac{d_c^o}{2D}\right). \quad (17)$$

Each of the drag force expressions just given involves a viscous contribution proportional to velocity and an inertial term expressed as a quadratic velocity dependence. To adapt to the deep-bed filtration context, these drag equations are recast as local functions of the local instantaneous values of the porosity and of the effective specific surface area of the collector + fines assemblage, a_{cf}. This latter term is used instead of the collector diameter because the effective specific surface area is prone to increase as fines are captured onto the surface of the collectors (Stephan and Chase, 2000; Ortiz-Arroyo et al., 2002). A constitutive relation accounting for the changes undergone by a_{cf} due to accumulation of fines will be provided later.

To represent the gas–fluid relative motion intervening in $F_{g\ell}$, the effect of slip between the gas and fluid is accounted for by means of the velocity u^* at the gas–liquid interface derived in Iliuta et al. (2002) and estimated from the slit model as

$$u^*=\frac{72}{E_1}\frac{\epsilon_\ell}{(1-\epsilon)^2a_{cf}^2\mu_\ell}\left[\frac{1}{2}\left(-\frac{\Delta P}{H}+\rho_\ell g\right)\epsilon_\ell+\left(-\frac{\Delta P}{H}+\rho_g g\right)\epsilon_g\right]. \quad (18)$$

$\psi_{g\ell}$ is a complex function that depends on the bed hydrodynamics and is incorporated to account for the enhancement of pressure drop due to the gas–liquid interactions in trickle flow.

Filtration Rate Model

In deep-bed filtration simulations, the logarithmic law of Iwasaki (1937) is typically used to express the relationship between the filtration rate and the specific deposit, σ, which represents the volume of fines deposited per unit reactor volume (Tien, 1989)

$$N(\sigma,c,t,z)=\lambda(\sigma)cu_\ell. \quad (19)$$

Equation 19 is among the simplest forms to express the dependence between the local filtration rate, the local fines concentration, and the local interstitial fluid velocity. It is assumed that it holds in the particular gas–liquid flow context of the low interaction trickle-flow regime being studied in this work. This assumes that the fluid flow field is affected only "hydrodynamically" by the presence of the flowing gas phase. In other words, the presence of gas is felt via the interstitial velocity, u_ℓ, which in turn affects the fluid holdup, ϵ_ℓ, and the fines concentration, c. Furthermore, the conditions of full bed wetness and of complete separation between flowing phases reinforce the similarity between the filtration in two-phase trickle flow and that occurring in classic single-phase flow deep-bed filtration.

In Eq. 19, λ represents the filter coefficient, or the probability for a fine to be captured as it travels a unit distance through the bed (Tien, 1989). The form of the filter coefficient is determined by the nature of the capture phenomena,

that is, (monolayer) fine–collector or (multilayer) fine–fine interactions. The capture of fines evolves thus through a two-step mechanism:

• Fine–collector capture step (initial stage): In the early moments of filtration, the almost clean porous bed exhibits a σ-independent filter coefficient, λ^o, as long as the critical specific deposit, σ_{cr}, that is, the amount of fines for completing a monolayer of coating, is not attained. The critical specific deposit can be estimated according to Choo and Tien (1995b) as

$$\sigma_{cr} = \left[\left(1+2\frac{d_f}{d_c^o}\right)^3 - 1\right](1-\epsilon_d)(1-\epsilon^o). \tag{20}$$

During the initial step, the fines adhere to the collector surface via fine–collector interaction forces. Beside the fluid drag, the gravitational, and the London–van der Waals surface-interactive forces, the Brownian diffusion force has to be accounted for, especially for submicron fines (Tien, 1989). Hence, when $\sigma \le \sigma_{cr}$, the correlation of Rajagopalan and Tien (1976) is used

$$\lambda^o = \frac{3}{2}\frac{\eta^o \sqrt[3]{1-\epsilon^o}}{d_c^o}, \tag{21}$$

in which η^o represents the initial collection efficiency given by

$$\eta^o = A_s^o(1-\epsilon^o)^{2/3}N_L^{1/8}N_R^{15/8} + 3.375\times10^{-3}A_s^o(1-\epsilon^o)^{2/3}N_G^{6/5}N_R^{-2/5} + 4\sqrt[3]{A_s^o}\,Pe^{-2/3}, \tag{22}$$

where $A_s^o = [2(1-p^5)]/w$ is the Happel parameter, $p = (1-\epsilon^o)^{1/3}$,

$$w = 2-3p+3p^5-2p^6 \tag{23}$$

all calculated at ϵ^o, and the dimensionless groups N_R, N_L, N_G, and Pe represent, respectively, the interception group, the London–van der Waals group, the gravitational group, and the Péclet number, based on the clean collector diameter d_c^o.

• Fine–fine capture step: Once $\sigma \ge \sigma_{cr}$, filtration becomes driven by the fine–fine interaction captures, yielding a multi–layer deposit for which the filter coefficient no longer remains constant in time. For fines subject in addition to Brownian motion, Tien et al. (1979) proposed the following correlation for representing the change of the filter coefficient as a function of the specific deposit

$$\frac{\lambda}{\lambda_o} = B_1\frac{A_s}{A_s^o}\left[1+\frac{\sigma}{(1-\epsilon^o)(1-\epsilon_d)}\right]^{17/24} + B_2\frac{A_s}{A_s^o}\left[1+\frac{\sigma}{(1-\epsilon^o)(1-\epsilon_d)}\right]^{4.4/3} + B_3\left(\frac{A_s}{A_{os}}\right)^{1/3}\left(\frac{1-\epsilon}{1-\epsilon^o}\right)^{2/3}\left[1+\frac{\sigma}{(1-\epsilon^o)(1-\epsilon_d)}\right]^{4/9}, \tag{24}$$

where

$$B_1 = (1-\epsilon^o)^{2/3}A_s^o(\eta^o)^{-1}N_L^{1/8}N_R^{15/8} \tag{25}$$

$$B_2 = 3.375\times10^{-3}(1-\epsilon^o)^{2/3}(\eta^o)^{-1}A_s^oN_G^{1.2}N_R^{-0.4} \tag{26}$$

$$B_3 = 4\sqrt[3]{A_s^o}\,(\eta^o)^{-1}Pe^{-2/3} \tag{27}$$

$$\frac{A_s}{A_s^o} = \left[\frac{1-(1-\epsilon)^{5/3}}{1-(1-\epsilon^o)^{5/3}}\right] \times\left[\frac{2-3(1-\epsilon^o)^{1/3}+3(1-\epsilon^o)^{5/3}-2(1-\epsilon^o)^2}{2-3(1-\epsilon)^{1/3}+3(1-\epsilon)^{5/3}-2(1-\epsilon)^2}\right]. \tag{28}$$

In Eqs. 25–27, η^o is the initial collection efficiency calculated from Eq. 22, and A_s is the Happel parameter corresponding to ϵ.

Constitutive Relation for the Effective Specific Surface-Area

With the progress of bed plugging, the solid–fluid surface area of the trickle bed is altered by two opposing phenomena (Stephan and Chase, 2000). The deposition of a fine particle onto the collector surface causes an increase in surface area by addition of the area portion of the particle exposed to the streamline flow ($\gamma\pi d_f^2$). Simultaneously a portion of the collector area, located beneath the anchored fine, and amounting to A_Δ, is lost by the collector due to the "shadow effect" brought about by the captured fine (Tien and Payatakes, 1979). The shadow effect refers to the fact that once a particle is captured by a collector, a fraction of the collector surface near the deposited particle is no longer accessible to additional approaching fines. The total effective surface area can be expressed as the summation of the number of particles (collector and fine) multiplied by the *true* surface area available for deposition on each particle. At every point of the computational space, the local and instantaneous effective specific surface area is expressed per unit total solid volume in grid cell as

$$a_{cf}(t,z) = \frac{N_c(z)\gamma\pi d_c^2(t,z) + N_c(z)\partial N_f(t,z)\left[\gamma\pi d_f^2 - A_\Delta(t,z)\right]}{N_c(z)\frac{\pi}{6}(d_c^o)^3 + N_f(t,z)\frac{\pi}{6}d_f^3}. \tag{29}$$

The first term in the numerator of Eq. 29 reflects the area contributed by the collectors and the second, the area of the fines that is available for further interception. Not all the geometrical area of the collectors and the deposited fines is available for momentum transfer. Thus, the geometrical parameter, γ, was introduced to account for the peripheral areas effectively involved in interception (Stephan and Chase, 2000; Ortiz-Arroyo et al., 2002).

The terms N_c and N_f are, respectively, the number of collectors and the number of captured fines in (differential) cell volume $\upsilon \propto dz$

$$N_c(z) = \frac{6\upsilon}{\pi(d_c^o)^3}(1-\epsilon^o) \tag{30}$$

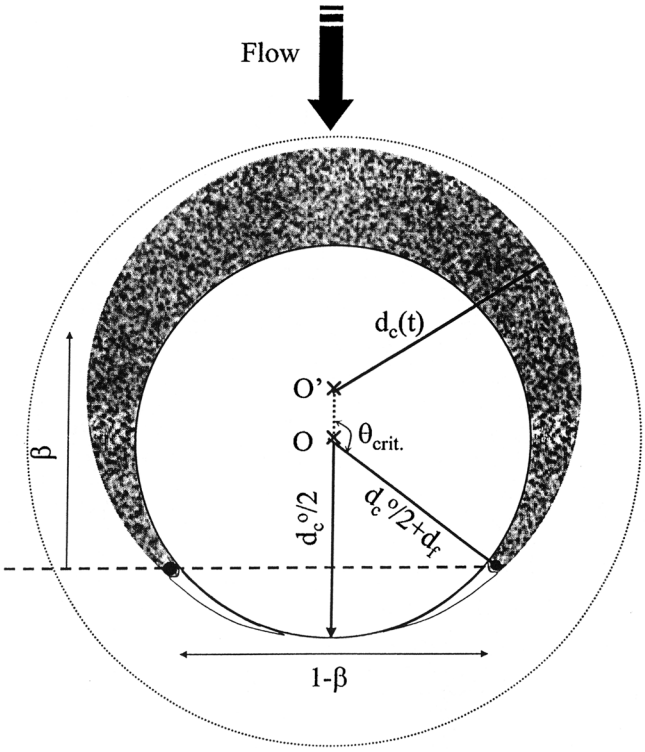

Figure 1. Sphere-in-cell representation of the fines' layer building up on top of collector for estimating the parameter β.

$$N_f(t,z) = \frac{6v}{\pi d_f^3}[\epsilon^o - \epsilon(t,z)](1-\epsilon_d). \tag{31}$$

∂N_f represents how many fines, per collector, culminate at the periphery of the collector + deposit assemblage at time, t [the peripheral fines populate the area corresponding to the cross-section fraction β; see Ortiz-Arroyo et al. (2002) for the other details of the model and Figure 1]

$$\partial N_f(t,z) = 4\beta(t,z)(1-\epsilon_d)\left[\frac{d_c(t,z)}{d_f}\right]^2, \tag{32}$$

where

$$\beta = 1 - \frac{A_H}{\pi d_c^2(t)} \tag{33}$$

$$A_H = \frac{\pi}{2}(d_c^o)^2(1+\cos\,\theta_{cr}) \tag{34}$$

$$\cos\,\theta_{cr} \approx -\frac{d_c(t,z)}{d_c(t,z)+2d_f}. \tag{35}$$

The collector area loss, A_Δ, occasioned by the shadow effect per attached fine is estimated from the shadow left by an equilateral triangle in which the fine is inscribed (Stephan and Chase, 2000)

$$A_\Delta(t,z) = \frac{d_c^2(t,z)}{8}\left[2\sqrt{3}\,\frac{d_f}{d_c(t,z)} - \sin\left(2\sqrt{3}\,\frac{d_f}{d_c(t,z)}\right)\right]. \tag{36}$$

To account for the nonuniform circumferential growth of the deposit on the collector surface, the increase in the collector diameter is calculated as a function of the specific deposit, assuming sphere-in-cell model configurations such as that of Choo and Tien (1995b)

$$\frac{d_c(t,z)}{d_c^o} = \sqrt[3]{1+\frac{\sigma(t,z)}{(1-\epsilon_d)(1-\epsilon^o)}}\,. \tag{37}$$

Method of Solution

To make the model (Eqs. 1–7) solvable, boundary and initial conditions need to be specified for the system in the trickle-flow regime. It is assumed that there is an inlet for gas and fluid at the top of the reactor and an outlet at its bottom. The pressure, the fines concentration, the liquid and gas holdups, and the gas and liquid interstitial velocities are specified at the inlet. The spatial discretization is performed using the standard cell-centered finite difference scheme. The GEAR integration method for stiff differential equations is used to integrate the time derivatives.

Transient flow simulations in a clean bed are first performed until the (pressure, velocity, and holdup) flow fields reach steady state. Under these circumstances, the conservation equations (Eqs. 8–12) are solved in the absence of fines in the liquid. Starting from these solutions, transient simulations with fines-containing liquid are then resumed by solving Eqs. 1–7.

Results and Discussion

Model parameters' estimation

To make the model equations (Eqs. 1–7) solvable, the Ergun constants, E_1 and E_2, the gas–liquid interaction factor, $\psi_{g\ell}$, and the surface-area parameter, γ, need to be specified. The Ergun single-phase flow parameters can be set either by measurements of single-phase pressure drops (Holub et al., 1992) or estimated from correlations (Iliuta et al., 1998) in the literature. Regarding the interaction parameter, $\psi_{g\ell}$, it is bounded within the range [1–10]. Under no interactions is it close to unity, whereas, at high pressure conditions, where the gas–liquid interactions are important, $\psi_{g\ell}$ can be as high as 10. This interaction function can be estimated using a correlation proposed by Iliuta et al. (2002). The surface-area parameter, γ, represents the percentage of a single-particle surface area available for momentum transfer. According to the simulation results, approximately 55% of the surface area is available for momentum transfer, and thus for particle capture. This value is in close agreement with previously recommended values proposed by Liu et al. (1995), Stephan and

Chase (2000), and Ortiz-Arroyo et al. (2002), which state that particle collisions mostly exploit the upper frontal hemisphere of collector and fine alike.

Experimental verification and simulations

Validation of the model for the capture of fines, the plugging of bed, and the buildup in pressure gradient is based on the experimental work of Gray et al. (2002). Ambient plugging tests (room temperature and atmospheric pressure) were run using kerosene as the liquid phase (seeded with kaolin fines of 0.7 μm) and air as the gas phase. Trilobe (Ni + Mo on γ-alumina) and spherical (γ-alumina) catalytic particles were used as collectors. The experimental conditions are listed in Table 1. Figures 2a and 2b shows the comparison between the experimental results, expressed as two-phase pressure-drop ratios $\Delta P/\Delta P^o$ vs. time, and the results obtained with the present model for the spherical and the trilobe collectors, respectively; and ΔP^o represents the steady-state pressure drop of the clean bed obtained from the solution of Eqs. 8–12. It can be seen that the predicted pressure buildup behavior is found to agree very well with physical reality for both catalyst types. During the course of deep-bed filtration, the fines are progressively retained on the catalyst particles, yielding in trickle flow up to a fourfold increase in pressure drop compared to the clean bed with no clay fines in the liquid stream.

Filtration in two-phase flow porous media systems being complex, flow-field imaging of the transient phenomena accompanying fluid flow and fines deposition in a bed is not trivial and has not been experimentally attempted yet. It is proposed here to test the model potentiality through simulations of different experimental configurations by solving the transport equations for the trickle flow deep-bed filtration. To illustrate the quantitative and qualitative features of the plugging trickle-flow regime, the simulated results shown below are presented (1) in terms of longitudinal profile snapshots of the local porosity and the fluid fines concentration, and (2) in the form of transient pressure-drop buildup at different fines diameters, liquid superficial velocities and viscosities, fines feed concentrations, gas superficial velocities and densities, and finally porosity of the deposit.

Figure 3 shows the effect of the fines diameter on the $\Delta P/\Delta P^o$ ratio. At a higher fines diameter, the interception dimensionless group is higher and the filtration rate is higher, yielding higher overall specific deposits at the same filtration time. As a result, the bed porosity decreases and the two-phase pressure drop increases. Because the fines deposition is more noticeable at high fines diameter, the following simulations were undertaken for these conditions.

Figures 4a and 4b are snapshots of the longitudinal profiles of porosity and correspondingly fines concentration in the liquid–solid suspension normalized, respectively, with respect to the initial uniform porosity, ϵ^o, and suspension feed concentration, c^o. Figure 4a shows that the extent of fines deposition depends strongly upon axial distance. There is a noticeable decrease in bed porosity in the first section of the catalyst bed in agreement with the decrease of fines concentration in the evolving suspension (Figure 4b). As time evolves, the plugging front progressively fills up the column. However, plugging is more confined in the entrance region.

When a liquid–solid suspension passes through a bed, some of the fines are retained by the bed, and the two-phase pressure drop increases compared to the clean bed with two-phase flow without fines (Figures 5a–5c). The major change resulting from particle deposition involves the effective porosity of the bed, and therefore the increase in two-phase pressure drop is the result of the decrease in the bed porosity.

The effect of the gas phase can be separated into the effect of the superficial gas velocity and of the reactor pressure (or gas density). A comparison of the plots of the pressure-drop ratios vs. volume-averaged specific deposit (Figures 5a and

Table 1. Model Parameters

Exp. Conditions (Gray et al., 2002)	Exp. Validation of the Model and Its Simulations
Properties of materials	*Properties of materials*
Liquid	Liquid
Kerosene	Kerosene
Vis.: 2mPa·s	Vis.: 1–2 mPa·s
Dens.: 801 kg/m^3	Dens.: 801 kg/m^3
Gas	Gas
Air	Air
Dens.: 1.3 kg/m^3	Dens.: 1.3–10.3 kg/m^3
Fines	Fines
Kaolinite	Kaolinite
Avg. dia.: 0.7 μm	Avg. dia.: 0.7 and 26 μm
Dens.: 2,000 kg/m^3	Dens.: 2,000 kg/m^3
Porosity of deposit layer:	Porosity of deposit layer: 0.75–0.8
0.80 (spherical particle)	(Tien, 1989; Gray et al., 2002)
0.74 (trilobe particle)	
Packing	Packing
1. Spherical catalyst particle	1. Spherical catalyst particle
Dia.: 0.004 m	Dia.: 0.004 m
Bed porosity: 0.385	Bed porosity: 0.385
2. Trilobe catalyst	
Effective dia.: 0.00129 m	
Bed porosity: 0.425	
Size of fixed-bed reactor	Geometry of fixed-bed reactor
Dia.: 0.038 m	Dia.: 0.038 m
Height: 0.9 m	Height: 0.9 m

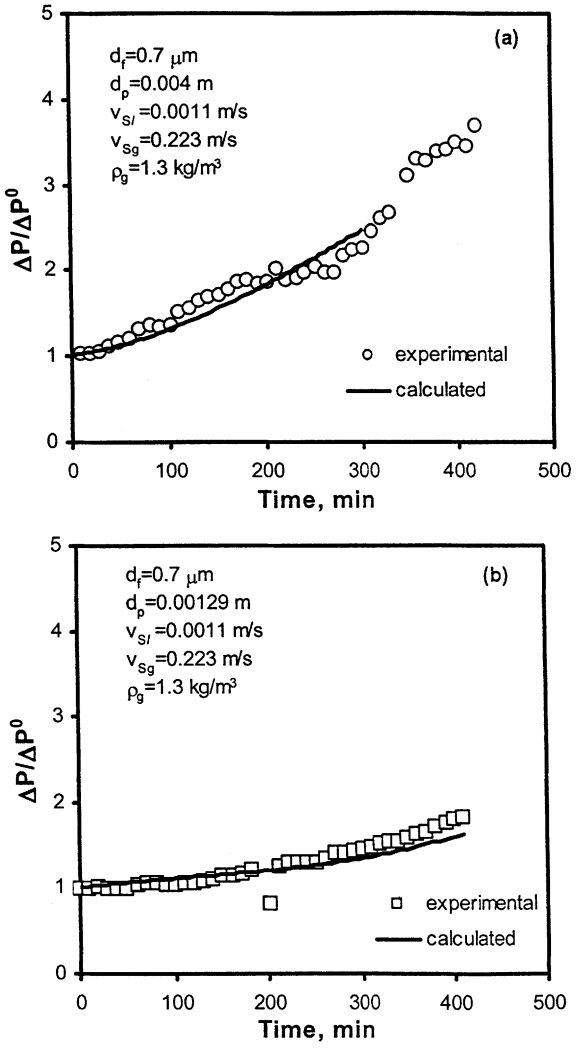

Figure 2. Representative plots of pressure buildup with time in trickle-flow reactors: (a) spherical catalyst; (b) trilobe catalyst (data from Gray et al., 2002).

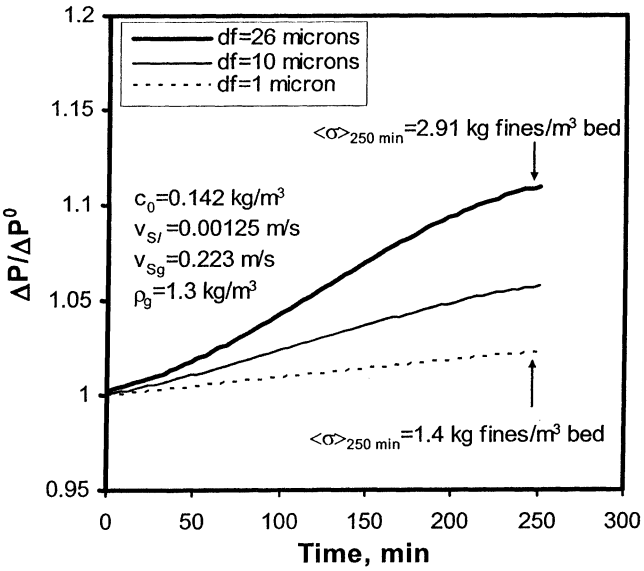

Figure 3. Two-phase pressure-drop ratio vs. time at different values of fines diameters.

5c) suggests that the influence of gas flow rate is not very important in the fines-deposition process. Similarly, a comparison of the predicted pressure-drop histories at different gas-density values (Figures 5b and 5c) indicates that, as in the case of the gas flow rate, ρ_g does not affect significantly the deposition process.

Higher liquid superficial velocities cause higher liquid holdups. It is instructive to see from Figure 6a (curves [1] and [2]) that for constant c_o the rise of pressure-drop buildup and of the volume-averaged (or overall) specific deposit, $\langle \sigma \rangle$, is steeper at higher liquid superficial velocity (or liquid holdup). This appears to be counterintuitive in regard to what one might expect from the deep-bed filtration behavior of single-phase flows. Under such circumstances, the bed is known to increasingly capture fines the lower the liquid superficial velocity or Reynolds number [see, for example, Narayan et al. (1997)], while the liquid holdup, which is equivalent to the bed porosity, has a tendency to decline, as a result of plugging, as time elapses. The situation is quite different in two-phase flow. A higher v_ℓ means a shorter residence time for each element in the suspension, resulting in a lower specific deposit, as should be expected from single-phase deep-bed filtration. Simultaneously, higher liquid holdups mean higher amounts of fines to impinge on the collector's surface, and thus conversely higher specific deposits are to be expected. As v_ℓ and ϵ_ℓ appear to exert opposite effects on the overall specific deposit, the net outcome may be case-dependent for the filtration performance. In the simulation of 26-μm fines shown in Figures 6a and 6b (curves [1] and [2]), the filtration performance, in terms of capture efficiency, grows worse the higher the liquid velocity. At $v_\ell = 3.1$ mm/s, the filtrate is indeed more loaded with fines (Figure 6b) even though the overall specific deposit is twice the corresponding value for $v_\ell = 1.2$ mm/s. This higher specific deposit in the former case also explains the higher pressure-drop ratios at $v_\ell = 3.1$ mm/s.

Moreover, keeping the quantity $c_o v_\ell$ constant, which measures the mass flux of fines entering the reactor (curves [1] and [2] in Figure 6c), yields virtually confounded pressure-drop ratios and ultimately identical values for the overall specific deposit. Also curves [1] (in Figure 6a) and [2] (in Figure 6c) show the effect of the inlet fines concentration on the $\Delta P/\Delta P^o$ ratio. At a higher fines concentration, the filtration rate is higher, giving higher overall specific deposits. As a result, the bed porosity decreases and the two-phase pressure drop increases.

Figure 7 indicates that the $\Delta P/\Delta P^o$ ratio decreases as the liquid viscosity increases. By impeding the migration of fines to the collector surface, more viscous liquids seem to yield lower values for the overall specific deposit, thus yielding less porosity reduction in the bed, and as a consequence lower two-phase pressure-drop ratios.

If the porosity, ϵ_d, of the deposit barely affects the overall specific deposit, a decrease in the value of ϵ_d means compacter deposits and a higher bed porosity, which logically

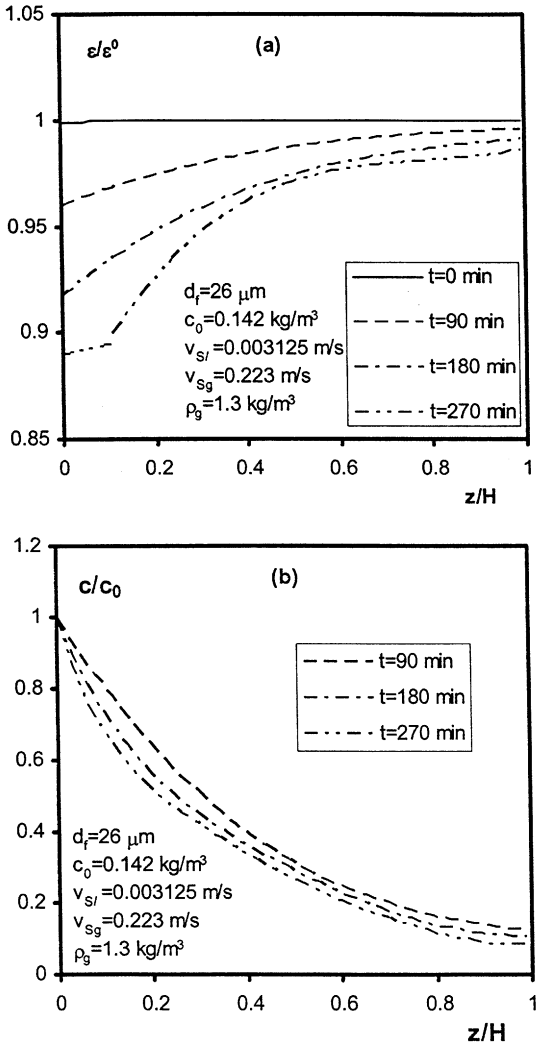

Figure 4. Longitudinal variations of (a) (normalized) bed porosity and (b) (normalized) fines concentration.

translates into a lower rise in the two-phase pressure-drop ratio (Figure 8).

Concluding Remarks

A 1-D transient two-fluid dynamic model based on the macroscopic volume-averaged mass and momentum balance equations and volume-averaged species balance equation for the fines was proposed to describe the two-phase flow and space-time evolution of the deposition of fines in trickle-flow reactors. The model assumed that plugging occurs via deep-bed filtration mechanisms. It further incorporated physical effects of porosity and effective specific surface-area changes due to the capture of fines, inertial effects of phases, and coupling effects between the fines filter rate equation and the interfacial momentum exchange force terms. Both monolayer and multiple-layer deposition mechanisms were accounted for during the developmental stages by including the appropriate filter-coefficient formulation.

This article is to be viewed as an inducement to explore experimentally in more detail the hydrodynamic effects for

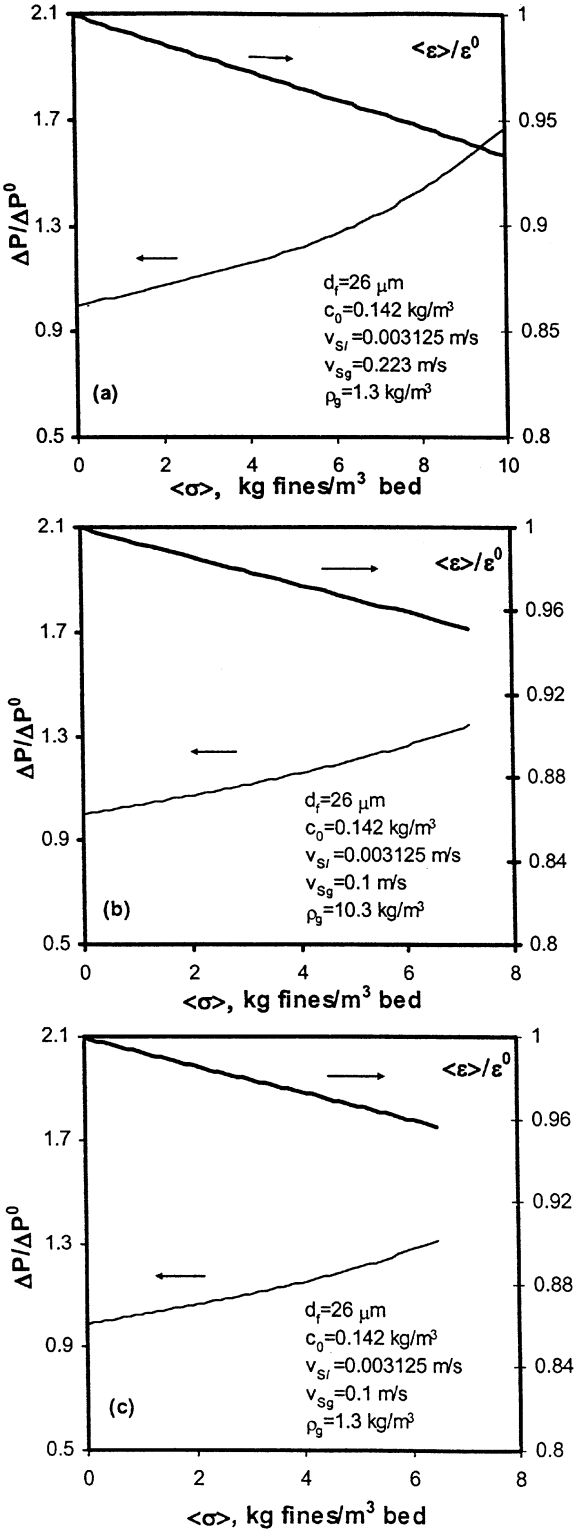

Figure 5. Total two-phase pressure-drop ratio and volume-averaged bed porosity vs. volume-averaged specific deposit.

this important category of multiphase flows. More experimental work on deep-bed filtration phenomena in trickle-flow reactors is recommended to understand their dependence on

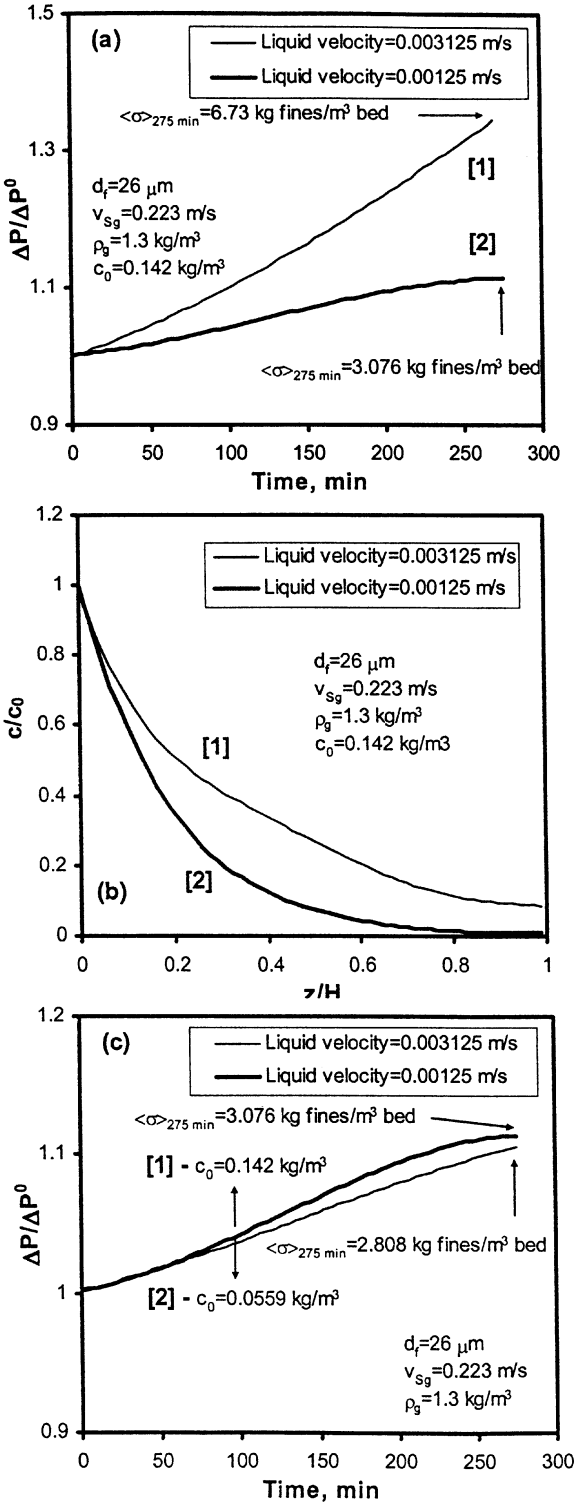

Figure 6. Impact of liquid superficial velocity on: (a, c) transient behavior of the two-phase pressure drop ratio and volume-averaged specific deposit; (b) (normalized) fines concentration longitudinal profiles at $t = 270$ min.

the flow and bed variables, as well as on the physicochemical phenomena taking place at the fines–collector interfaces. It is felt that space-resolved imaging techniques such as magnetic resonance imaging or nuclear-radiation-based tomography are very suitable and powerful experimental tools for this class of slowly evolving flows (no necessity for high time resolution). It is recommended that these tools be employed to further our fundamental knowledge of these gas–liquid–solid–solid systems, and to validate and help improving the theoretical models needed for scale-up of trickle beds in the presence of bed plugging.

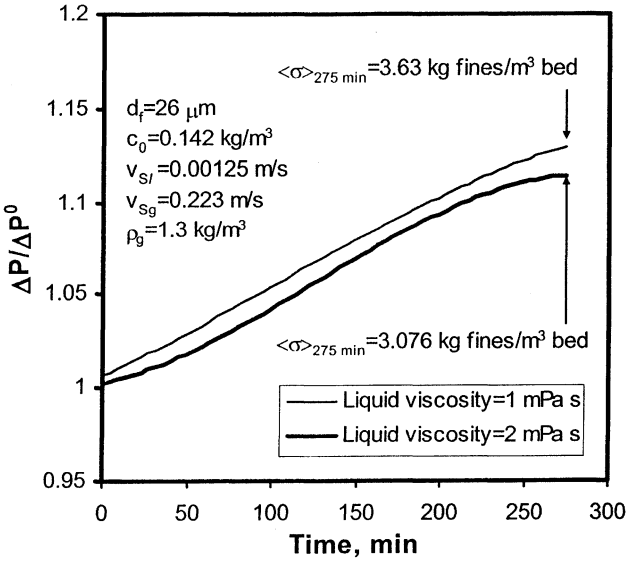

Figure 7. Two-phase pressure-drop ratio vs. time at different liquid viscosity.

Acknowledgments

The authors thank the following institutions for their financial contributions: The Natural Sciences and Engineering Research Council of Canada, the Fonds pour la formation de chercheurs et d'aide à la recherche (Québec).

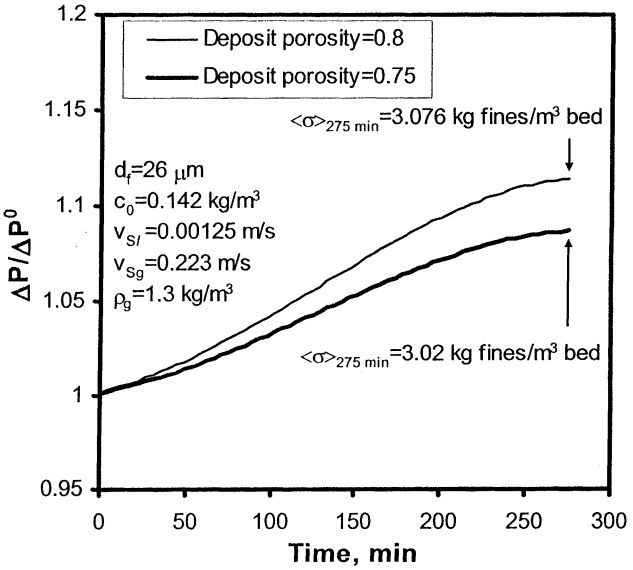

Figure 8. Two-phase pressure-drop ratio vs. time for deposits exhibiting different values of porosity, ϵ_d.

Notation

a_{cf} = effective specific surface area, m^{-1}
A_H = hidden area in downstream collector pole, m^2
A_Δ = shadow-area loss, m^2
c = fine volumetric concentration (liquid volume basis)
d = particulate effective diameter (collector or fine), m
D = column diameter, m
D_{BM} = Brownian diffusion coefficient, $D_{BM} = 2k_BT/6\pi\mu_\ell d_f$, m^2/s
E_1, E_2 = Ergun constants
$F_{g\ell}$ = gas–liquid drag force, N/m^3
$F_{\ell s}$ = liquid–solid drag force, N/m^3
g = gravitational acceleration, m/s^2
G = gas mass flux, $kg/m^2 \cdot s$
H = Hamaker constant, J or bed height, m
k_B = Boltzmann constant, J/K
N = filtration rate (reactor volume basis), s^{-1}
N_c = number of collector in grid-cell volume, υ
N_f = number of trapped fines in grid-cell volume, υ
∂N_f = number of peripheral fines per collector
N_G = gravitational dimensionless group, $N_G = [(\rho_f - \rho_\ell)d_f^2 g]/18\mu_\ell u_\ell$
N_L = London–van der Waals dimensionless group, $N_L = 4H/9\pi\mu_\ell d_f^2 u_\ell$
N_R = interception dimensionless group, $N_R = d_f/d_c^o$
P = pressure, Pa
Pe = Brownian diffusion group, $Pe = [d_c(t)u_\ell]/\epsilon_\ell D_{BM}$
T = temperature, K
u_α = average interstitial velocity of α-fluid, m/s
u^* = interfacial velocity, m/s
υ = grid-cell volume, m^3
υ_α = α-phase superficial velocity, m/s

Greek letters

β = collector cross-section fraction
ϵ = grid-cell, bed, or deposit porosity
$\langle\epsilon\rangle$ = bed volume-averaged porosity
ϵ_g = gas holdup
ϵ_ℓ = liquid holdup
γ = fine cross-section fraction
η = collector efficiency
λ = filter coefficient, m^{-1}
λ_0 = clean filter coefficient, m^{-1}
μ_α = α-phase dynamic viscosity, $kg/m \cdot s$
μ_α^e = α-phase effective viscosity (combination of bulk and shear terms), $kg/m \cdot s$
θ_{cr} = angle of critical point of deposition
ρ_α = density of α phase, kg/m^3
σ = specific deposit (reactor volume basis), $\sigma = (\epsilon^o - \epsilon)(1 - \epsilon_d)$
$\langle\sigma\rangle$ = bed volume-averaged specific deposit, $\langle\sigma\rangle = H^{-1}\int_0^H \sigma(t)\,dz$
$\psi_{g\ell}$ = gas–liquid interaction factor

Subscripts and superscripts

c = collector
crit. = critical
d = deposit
f = fine
g = gas
ℓ = liquid
o = clean-bed state
s = solid

Literature Cited

Attou, A., C. Boyer, and G. Ferschneider, "Modelling of the Hydrodynamics of the Cocurrent Gas-Liquid Trickle Flow Through a Trickle-Bed Reactor," *Chem. Eng. Sci.*, **54**, 785 (1999).

Choo, C.-U., and C. Tien, "Simulation of Hydrosol Deposition in Granular Media," *AIChE J.*, **41**, 1426 (1995a).

Choo, C.-U., and C. Tien, "Analysis of the Transient Behavior of Deep-Bed Filtration," *J. Colloid Interface Sci.*, **169**, 13 (1995b).

Dankworth, D. C., I. G. Kevrekidis, and S. Sundaresan, "Dynamics of Pulsing in Trickle Beds," *AIChE J.*, **36**, 605 (1990).

Fourar, M., R. Lenormand, and F. Larachi, "Extending the *F*-Function Concept to Two-Phase Flow in Trickle Beds," *Chem. Eng. Sci.*, **56**, 5987 (2001).

Gray, M. R., N. Srinivasan, and J. H. Masliyah, "Pressure Buildup in Gas-Liquid Flow Through Packed Beds Due to Deposition of Fine Particles," *Can. J. Chem. Eng.*, **80**, 346 (2002).

Herzig, J. P., D. M. Leclerc, and P. Le Goff, "Flow of Suspensions Through Porous Media: Application to Deep Bed Filtration," *Ind. Eng. Chem.*, **62**, 8 (1970).

Holub, R. A., M. P. Dudukovic, and P. A. Ramachandran, "A Phenomenological Model of Pressure Drop, Liquid Holdup and Flow Regime Transition in Gas-Liquid Trickle Flow," *Chem. Eng. Sci.*, **47**, 2343 (1992).

Iliuta, I., F. Larachi, and B. P. A. Grandjean, "Pressure Drop and Liquid Hold-Up in Trickle Flow Reactors: Improved Ergun Constants and Slip Correlations for the Slit Model," *Ind. Eng. Chem. Res.*, **37**, 4542 (1998).

Iliuta, I., F. Larachi, and M. H. Al-Dahhan, "Double-Slit Model for Partially Wetted Trickle Flow Hydrodynamics," *AIChE J.*, **46**, 597 (2000).

Iliuta, I., B. P. A. Grandjean, and F. Larachi, "New Mechanistic Film Model for Pressure Drop and Liquid Holdup in Trickle Flow Reactors," *Chem. Eng. Sci.*, **57**, 3359 (2002).

Iwasaki, T., "Some Notes on Sand Filtration," *J. Amer. Water Works Assoc.*, **29**, 1591 (1937).

Le Page, J. F., S. G. Chatila, and M. Davidson, *Raffinage et Conversion des Produits Lourds du Pétrole*, Éditions Technip., Paris (1990).

Liu, S., A. Afacan, and J. Masliyah, "Steady Incompressible Laminar Flow in Porous Media," *Chem. Eng. Sci.*, **21**, 3565 (1994).

Liu, D., P. R. Johnson, and M. Elimelech, "Colloid Deposition Dynamics in Flow Through Porous Media," *Environ. Sci. Technol.*, **29**, 2963 (1995).

Meyers, R. A., *Handbook of Petroleum Refining Processes*, 2nd ed., McGraw-Hill, New York (1996).

Narayan, R., J. R. Coury, J. H. Masliyah, and M. R. Gray, "Particle Capture and Plugging in Packed-Bed Reactors," *Ind. Eng. Chem. Res.*, **36**, 4620 (1997).

O'Melia, C. R., and W. Ali, "The Role of Retained Particles in Deep Bed Filtration," *Prog. Water Technol.*, **10**, 167 (1978).

Ortiz-Arroyo, A., F. Larachi, B. P. A. Grandjean, and S. Roy, "CFD Modeling and Simulation of Clogging in Packed Beds with Non-aqueous Media," *AIChE J.*, **48**, 1596 (2002).

Propp, R. M., P. Colella, W. Y. Crutchfield, and M. S. Day, "A Numerical Model for Trickle Bed Reactors," *J. Comput. Phys.*, **165**, 311 (2000).

Rajagopalan, R., and C. Tien, "Trajectory Analysis of Deep Bed Filtration with the Sphere-in-Cell Porous Media Model," *AIChE J.*, **22**, 523 (1976).

Sáez, A. E., and R. G. Carbonell, "Hydrodynamic Parameters for Gas-Liquid Cocurrent Flow in Packed-Beds," *AIChE J.*, **31**, 52 (1985).

Stephan, E. A., and G. G. Chase, "Development of Volume-Average Theory for Deep-Bed Filtration," *AIChE J.*, **46**, 1918 (2000).

Tien, C., and A. C. Payatakes, "Advances in Deep Bed Filtration," *AIChE J.*, **25**, 737 (1979).

Tien, C., R. M. Turian, and H. Pendse, "Simulation of the Dynamic Behavior of Deep Bed Filters," *AIChE J.*, **25**, 385 (1979).

Tien, C., *Granular Filtration of Aerosols and Hydrosols*, Ser. in Chemical Engineering, Butterworths-Heinemann, Boston (1989).

Vigneswaran, S., and R. V. Tulachan, "Mathematical Modeling of Transient Behaviour of Deep Bed Filtration," *Water Res.*, **22**, 1093 (1988).

Wang, S., K. H. Chung, J. H. Masliyah, and M. R. Gray, "Deposition of Fine Particles in Packed Beds at Hydrotreating Conditions: Role of Surface Chemistry," *Ind. Eng. Chem. Res.*, **38**, 4878 (1999).

Wang, S., K. H. Chung, and M. R. Gray, "Role of Hydrotreating Products in Deposition of Fine Particles in Reactors," *Fuel*, **80**, 1079 (2001).

Whitaker, S., "The Transport Equations for Multi-Phase Systems," *Chem. Eng. Sci.*, **28**, 139 (1973).

Manuscript received Feb. 22, 2002, and revision received July 18, 2002.